Journal of Oceanography, Vol. 61, pp. 369 to 378, 2005

An Amplification Mechanism of Intraseasonal Long Rossby Wave in Subtropical Ocean

XIAOPEI LIN*, DEXING WU, QIANG LI and JIAN LAN

Key Laboratory of Physical Oceanography (Ocean University of China, Ministry of Education), Qingdao 266003, P.R. China

(Received 4 April 2004; in revised form 20 April 2004; accepted 22 June 2004)

The satellite altimeter data reveal that intraseasonal long Rossby wave is amplified in the western part of subtropical ocean. Based on a two and half layer ocean model we infer that the intraseasonal long Rossby wave may be amplified by the baroclinic instability. According to the baroclinic instability criterion derived from the two and half layer model, we calculate the baroclinic instability area of the Subtropical North Pacific Ocean based on Levitus98 data. The baroclinic instability area is well in accord with the amplification area of the intraseasonal long Rossby wave, and this also proves that the baroclinic instability is the main amplification mechanism of the intraseasonal long Rossby wave in the subtropical ocean. The consistency between the baroclinic instability area and potential vorticity (PV) pool is further proved in this paper, therefore, we have confidence that the intraseasonal long Rossby wave is amplified in the PV pool. Due to the relatively large ocean basin and weak ventilation, the PV pool is much larger in the North Pacific Ocean than in the North Atlantic Ocean, and this is the reason for the difference of wave amplification areas of these two Oceans.

Keywords:
· Long Rossby wave,
· baroclinic instability,
· PV pool.

1. Introduction

Long Rossby waves are the main mechanism in the cases when information about one part of the ocean is transferred to another part, or a non-equilibrium ocean state adjusts to an equilibrium one. In a recent study, Chelton and Schlax (1996) conducted a thorough analysis of the satellite altimeter data from the first 3-year TOPEX/POSEIDON mission and they found two interesting properties of the intraseasonal long Rossby wave. Firstly, the intraseasonal long Rossby wave seemed to be amplified abruptly in the western part of subtropical North Pacific Ocean (see Fig. 1). Secondly, the observed propagating speed of the intraseasonal long Rossby wave appeared to be faster than those predicted by the linear theory of first mode baroclinic free long Rossby wave out of the 10°S and 10°N.

Many studies also showed that the intraseasonal long Rossby wave was very obvious in the western part of the subtropical ocean (Mitchum, 1995; Liu and Wang, 1999; Hu and Liu, 2002; Chen *et al*., 2003; Qiao *et al*., 2004). Fu and Qiu (2002) found that the long Rossby wave, reflected in the eastern boundary, existed only in a limited area, from 3000–4000 km in 10°N to 200–300 km in 50°N, and this could prove that the intraseasonal long Rossby wave in the western part of the subtropical ocean should be amplified in the ocean.

Theories have been put forward by using a variety of mechanisms to explain the long Rossby wave speedup (Qiu *et al*., 1997; Killworth *et al*., 1997; White *et al*., 1998; De Szoeke and Chelton, 1999). But there are very few relevant studies for the amplification mechanism of the intraseasonal long Rossby wave in the subtropical Ocean. Based on the Rossby wave porpagation in 21°N, 32°N and 39°N (see Fig. 1), Chelton and Schlax (1996) thought that the topography may be the source of the intraseasonal long Rossby wave. They pointed out that in the 21°N the intraseasonal long Rossby wave seemed to be amplified in the Hawaii ridge, in the 32°N the intraseasonal long Rossby wave was amplified in the HESS ridge at about 175°W, and there were no obvious wave signals in the east of HESS ridge.

Is the topography the main amplification mechanism of the intraseasonal long Rossby wave? There are several things that do not support Chelton's view. Firstly, the amplification area of the intraseasonal long Rossby wave

* Corresponding author. E-mail: linxiaop@mail.ouc.edu.cn

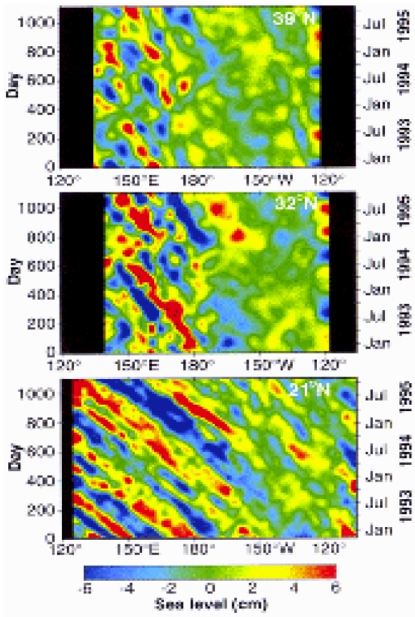

Fig. 1. Time-longitude sections of specifically filtered sea level at 21°N (upper), 32°N (middle) and 39°N (lower) (from Chelton and Schlax, 1996).

is not well agreed with the topography. Figure 2(a) is the distritution of sea level anomaly derived from altimeter data and Fig. 2(b) is the distribution of wave energy calculated based on the altimeter data from Stammer (1997), which can show the amplification area of the intraseasonal long Rossby wave. From Fig. 2 we can see that in the subtropical North Pacific Ocean the amplification area is not well agreed with the topography such as the Hawaii ridge and the HESS ridge. Moreover, although there exits the mid ocean ridge in the middle of the North Atlantic Ocean, the amplification area of the intraseasonal long Rossby wave is limited in a very small area near the western boundary, far away from the major topography. Secondly, the amplification area of the intraseasonal long Rossby wave is changeable with time. Figure 3 is the time-longitude section of sea level anomaly at 21°N, derived from 10 years TOPEX/POSEIDON altimeter data. From Fig. 3 we can see that in 1996 the intraseasonal long Rossby wave appeared in about 210°E and in 1998 the intraseasonal long Rossby wave was amplified in about 180°E. This means that the amplification area of the intraseasonal long Rossby wave is not in a fixed area and the mechanism of topography can not interpret this.

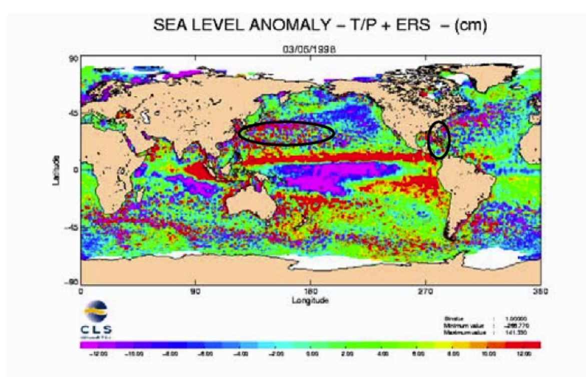

(a) Distribution of sea level anomaly in 03/06/1998.

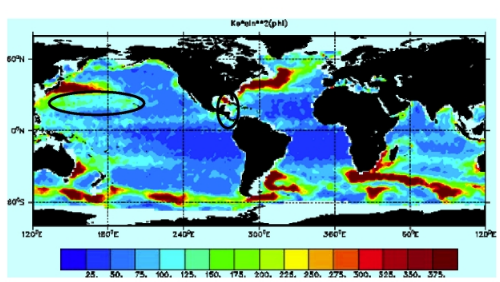

(b) Distribution of wave energy calculated by altimeter data from the first 3-year TOPEX/POSEIDON mission. (From Stammer, 1997)

Fig. 2. The distribution of wave amplification area from (a) sea level anomaly and (b) wave energy. The black circle in (a) and (b) show the amplification area of intraseasonal long Rossby wave.

Therefore, we can see that the amplification mechanism of the intraseasonal long Rossby wave in the subtropical ocean is still not clear. In this paper we will focus on the amplification mechanism of the intraseasonal long Rossby wave. Furthermore, we will try to use the new amplification mechanism to answer why the wave amplification area in the North Pacific Ocean is very large, but it is small in the North Atlantic Ocean as shown in Fig. 2.

Because of the limition of satellite orbit resolution, the altimeter data could not resolve the introseasonal long Rossby wave in the high latitude. Our study here is only in the subtropical ocean between 30°N and 30°S.

2. The Intraseasonal Long Rossby Wave in a Two and Half Layer Model

Two and half layer model has been widely used to study the ocean dynamics (Pedlosky, 1987, 1996; Liu, 1999a, b; Qiu, 1999). Although it is very simple, it can clearly highlight the main physical process. In this section we will also use the two and half layer model to study the possible amplification mechanism of the intraseasonal long Rossby wave.

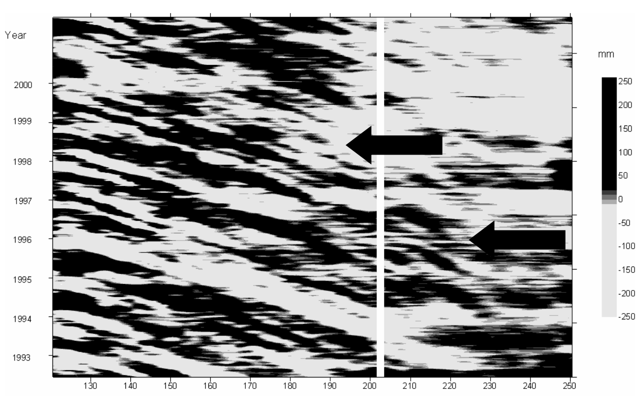

Fig. 3. Time-longitude sections of specifically filtered sea level at 21°N from 10 years TOPEX/POSEIDON altimeter data. The black arrows show the appearance of intraseasonal long Rossby wave.

First of all, we should make it clear if the observed intraseasonal long Rossby wave in the western part of the subtropical ocean is the forced Rossby wave or the free Rossby wave. Liu (1999a, b) has studied the forced Rossby wave using the two and half layer model. In his study Liu proved that the anomalies of wind stress curl mainly caused the first mode baroclinic Rossby wave, and the buoyancy anomalies mainly caused the second mode baroclinic Rossby wave. Because the Rossby wave, observed by altimeter data, is the first mode baroclinic Rossby wave, we can only check the wind forcing to know if the intraseasonal long Rossby wave is the forced Rossby wave or the free Rossby wave. According to Liu (1999a, b), the frequency of the forced Rossby wave should be determined by the forcing. This means that if the wind forcing causes the intraseasonal long Rossby wave, there should be an intraseasonal peak in the wind forcing frequency spectrum. Figures 4(a) and (b) is the frequency spectrum of wind stress curl in the western subtropical North Pacific Ocean, derived from the ERS satellite wind and the ECMWF wind. From Fig. 4 we can see that there is no intraseasonal peak in the frequency spectrum, so the observed intraseasonal long Rossby wave is the free wave and we can use the free wave model to study it.

We consider the ocean is composed of two active layers and an abyssal stationary layer. In the first layer the thickness is H_1, the averaged potential density is ρ_1, the background latitudinal mean flow is U_1. In the second layer the thickness is H_2, the averaged potential density is ρ_2, the background latitudinal mean flow is U_2. In the third layer the thickness is infinity, the average potential density is ρ_3 and there is no motion in this layer. The first layer represents the mixing layer or the seasonal theromalcline and the second layer represents the main theromalcline. Referencing to Pedlosky (1987, 1996), Qiu (1999), Liu *et al.* (2001) and Liu and Pan (2003), the quasigeostrophic PV equations are as follows

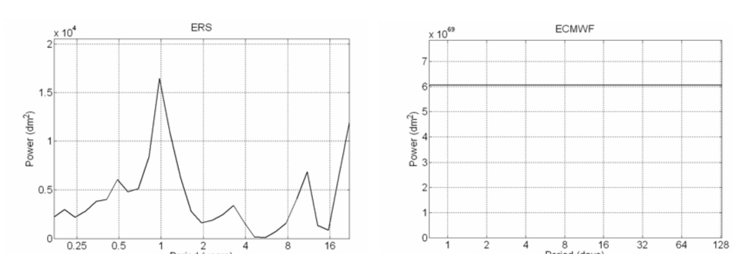

(a) ERS wind (b) ECMWF wind

Fig. 4. The frequency spectrum of wind stress curl from ERS wind (a) and ECMWF wind (b).

$$\left(\frac{\partial}{\partial t}+U_1\frac{\partial}{\partial x}\right)\left[\nabla^2\phi_1-F_1(\phi_1-\phi_2)\right]+\frac{\partial\pi_1}{\partial y}\frac{\partial\phi_1}{\partial x}=A_h\nabla^4\phi_1,$$

$$\left(\frac{\partial}{\partial t}+U_2\frac{\partial}{\partial x}\right)\left[\nabla^2\phi_2+F_2(\phi_1-\phi_2-r\phi_2)\right]+\frac{\partial\pi_2}{\partial y}\frac{\partial\phi_2}{\partial x}$$
$$=A_h\nabla^4\phi_2. \tag{1}$$

In these equations ϕ_1 and ϕ_2 are the perturbation stream functions in the first and second layers π_1 and π_2 and are the averaged PV in the first and second layers. A_h is the dispersion coefficient and in the ocean it is usually 500–2500 m/s (Qiu *et al.*, 1997).

Where

$$F_2=\frac{1}{r\lambda^2},\quad F_1=\frac{1}{\delta r\lambda^2},\quad \delta=\frac{H_1}{H_2},\quad r=\frac{\rho_2-\rho_1}{\rho_3-\rho_2},$$
$$\lambda=\frac{1}{f_0}\sqrt{\frac{(\rho_3-\rho_2)gH_2}{\rho_0}},\quad \pi_{1y}=\frac{\partial\pi_1}{\partial y}=\beta+F_1(U_1-U_2),$$
$$\pi_{2y}=\frac{\partial\pi_2}{\partial y}=\beta+F_2(U_2+rU_2-U_1). \tag{2}$$

If we do not consider the variations of meridianal mean flow and wavenumber, and only focus on the latitudinal propagating Rossby wave, we can set the perturbation solution as follows

$$\phi_n=R_eA_ne^{i(kx-kct)}\quad (n=1,2), \tag{3}$$

where k is the latitudinal wavenumber and c is the propagating phase speed. We set

$$P=k^2+F_1,\quad Q=k^2+F_2(1+r),\quad \sigma=ik^3A_h.$$

Combining Eq. (3) with Eq. (1), we can get

$$\left[(c-U_1)P+\pi_{1y}\right]A_1+(U_1-c)F_1A_2+\sigma A_1=0, \tag{4}$$

$$\left[(c-U_2)Q+\pi_{2y}\right]A_2+(U_2-c)F_2A_1+\sigma A_2=0. \tag{5}$$

For the none zero A_1 and A_2, it is required that the coefficient matrix of Eqs. (4) and (5) should be zero, we can get the eigenvalue problem

$$c^2+\frac{\left[P(\sigma+\pi_{2y})+Q(\sigma+\pi_{1y})-(PQ-F_1F_2)(U_1+U_2)\right]c}{PQ-F_1F_2}$$
$$+\frac{\left[(PQ-F_1F_2)U_1U_2+(\sigma+\pi_{1y})(\sigma+\pi_{2y})-PU_1(\pi_{2y}+\sigma)-QU_2(\pi_{1y}+\sigma)\right]}{PQ-F_1F_2}=0. \tag{6}$$

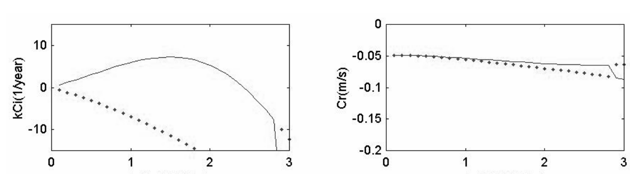

(a) The growth rate (b) The phase speed

Fig. 5. The relation of growth rate and phase speed as the function of wave number k.

Long Rossby wave dispersion relation can be derived from Eq. (6). Equation (6) has complex coefficients, so we can get the phase speed c_r and the growth rate kc_i. To determine the parameters, used in these equations, as an example we choose the subtropical Pacific Ocean between 25°N and 30°N. In this area the intraseasonal long Rossby wave is amplified in the west of 180°E. For the parameters f_0 and β the values associated with 28°N are used and other parameters are determined based on the Levitus98 data. The background mean flow U_1 and U_2 are calculated with an improved P-Vector method (Chu *et al.*, 2001). All the parameters are shown in Table 1.

On the basis of Eq. (6) and parameters in Table 1, the growth rate kc_i, phase speed c_r and wavenumber k are calculated. Figure 5 shows the relation among the growth rate kc_i, phase speed c_r and wavenumber k. It can be seen from Fig. 5(a) that the waves with wavenumber k larger than 2.5×10^{-5} (corresponding to the wavelength shorter than about 250 km) are the damping waves and the waves with wavenumber k smaller than 2.5×10^{-5} (corresponding to the wavelength longer than about 250 km) are the growing waves. The most instability wave has the wavenumber k = 1.2×10^{-5} m^{-1}, corresponding to the

Table 1. Parameters used in the two and half layer model.

Parameters	f_0 (s^{-1})	β ($s^{-1}m^{-1}$)	U_1 (ms^{-1})	U_2 (ms^{-1})	$\overline{H_1}$	$\overline{H_2}$ (m)	ρ_1 (σ_θ)	ρ_2 (σ_θ)	ρ_3 (σ_θ)
Climatic values	6.8×10^{-5}	2.0×10^{-11}	–0.15	–0.05	150	600	24.0	26.5	27.75

Table 2. The order of parameters.

Parameters	U_1, U_2, c_r, c_i	A_h	$H_{1,2}$	F_1, F_2	β	f_0	k
Order	$o(10^{-1})$	$o(10^2–10^3)$	$o(10^2–10^3)$	$o(10^{-10}–10^{-11})$	$o(10^{-11})$	$o(10^{-5})$	$o(10^{-5})$

wavelength about 523 km. The most instability wave has a phase speed of –5.64 cm/s and a period of 107 days (see Fig. 5(b)). The properties of the most instability wave are agreed well with those of the observed intraseasonal long Rossby wave (Chelton and Schlax, 1996; Chen, 2003; Qiao *et al.*, 2004) in 25°N–30°N.

From above we can infer that the baroclinic instability may be the amplification mechanism of the intraseasonal long Rossby wave in the subtropical ocean.

3. The Evidence of Baroclinic Instability Being the Amplification Mechanism of the Intraseasonal Long Rossby Wave in the Subtropical Ocean

In Section 2 we find that in the two and half layer model the intraseasonal long Rossby wave may be amplified by the baroclinic instability. But in the real ocean, is the baroclinic instability the amplification mechanism of intraseasonal long Rossby wave? In this section we will prove the consistency of wave amplification area with the baroclinic instability area in the subtropical ocean.

3.1 The baroclinic instability criterion

To get the baroclinic instability area in the subtropical ocean, we should first derive the baroclinic instability criterion. Our criterion is based on the two and half layer model used in Section 2.

$$(4)\times\frac{A_1H_1}{(U_1-c)}+(5)\times\frac{A_2H_2}{(U_2-c)},$$

we can get

$$k^2\left(H_1A_1{}^2+H_2A_2{}^2\right)+\frac{H_2}{r\lambda^2}\left(A_1-A_2\right)^2+\frac{H_2}{\lambda^2}A_2 =\frac{H_1\left(\pi_{1y}+\sigma\right)A_1{}^2}{\left(U_1-c\right)}+\frac{H_2\left(\pi_{2y}+\sigma\right)A_2{}^2}{\left(U_2-c\right)}. \quad (7)$$

In Eq. (7), it is required that the real and imaginary parts of the both sides should be equal, so

$$\frac{H_1A_1^2\left[\pi_{1y}c_i+\left(U_1-c_r\right)A_hk^3\right]}{\left|U_1-c\right|^2}i +\frac{H_2A_2^2\left[\pi_{2y}c_i+\left(U_2-c_r\right)A_hk^3\right]}{\left|U_2-c\right|^2}i=0. \quad (8)$$

The criterion for Eq. (8) demands

$$\left[\pi_{1y}c_i+\left(U_1-c_r\right)A_hk^3\right]\left[\pi_{2y}c_i+\left(U_2-c_r\right)A_hk^3\right]\prec 0. \quad (9)$$

This is the baroclinic instability criterion. For the intraseasonal long Rossby wave in the subtropical ocean, we can estimate the orders of all the parameters in (9).

According to Table 2 we can get

$$\pi_{1y}c_i,\pi_{2y}c_i\rightarrow o\left(10^{-12}\right),$$
$$\left(U_1-c_r\right)A_hk^3,\left(U_2-c_r\right)A_hk^3\rightarrow o\left(10^{-13}-10^{-14}\right).$$

This means that the dissipation term in Eq. (9) can be neglected, when we study the long wave, and the baroclinic instability criterion is mainly determined by the meridianal PV gradient π_{1y} and π_{2y}. The criterion of Eq. (9) can be simplified to

$$\pi_{1y}\pi_{2y}\prec 0. \quad (10)$$

This is the final baroclinic instability criterion and is agreed with Qiu (1999), when he studied the unstable wave in the subtropical-counter-current in the North Pacific Ocean.

3.2 *The consistency of baroclinic instability area with the wave amplification area in the subtropical ocean*

According to the criterion (10), we can determine the baroclinic instability area in the subtropical ocean by calculating π_{1y} and π_{2y} based on the Levitus98 data. If we use Eq. (2) to calculate π_{1y} and π_{2y}, we should know the background mean flow U_1 and U_2 first. No matter which method we use to calculate the mean flow based on the Levitus98 data, we cannot avoid the error induced by introducing an artificially stationary reference layer. In this section we will use another method to calculate π_{1y} and π_{2y}.

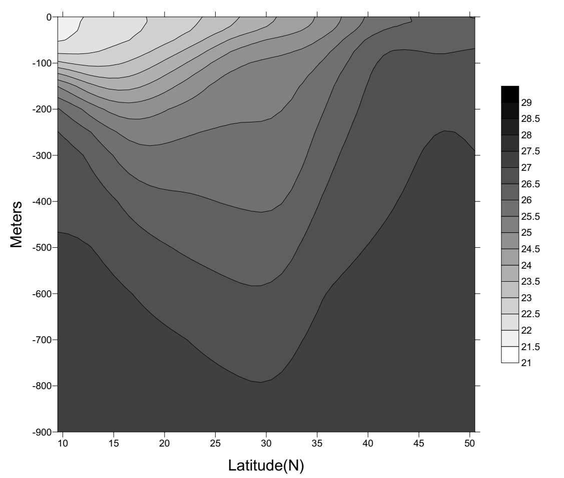

Fig. 6. The potential density field in the 160°E section in the North Pacific Ocean.

According to Pedlosky (1996), the PV in the first layer can be expressed as f/H_1. We calculate the meridianal gradient of PV in the first layer and get:

$$\frac{\partial}{\partial y}\left(\frac{f}{H_1}\right)=\frac{\beta}{H_1}-\frac{f_0}{H_1^2}\frac{\partial H_1}{\partial y}=\frac{1}{H_1}\left(\beta-\frac{f_0}{H_1}\frac{\partial H_1}{\partial y}\right). \quad (11)$$

H_1 is the thickness of the first layer. The "thermal wind" relation gives

$$U_1-U_2=-\frac{(\rho_2-\rho_1)g}{f_0\rho_0}\frac{\partial H_1}{\partial y}. \quad (12)$$

Combining Eqs. (11) with (12) we can get

$$\frac{\partial}{\partial y}\left(\frac{f}{H_1}\right)=\frac{1}{H_1}\left[\beta+F_1(U_1-U_2)\right]=\frac{\pi_{1y}}{H_1}.$$

So we can get π_{1y} and π_{2y} by calculating the meridianal gradient of PV (f/H_n, n = 1, 2). In this way, we can avoid calculating the background mean flow and

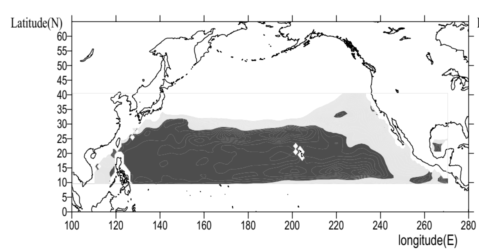

(a) Baroclinic instability area

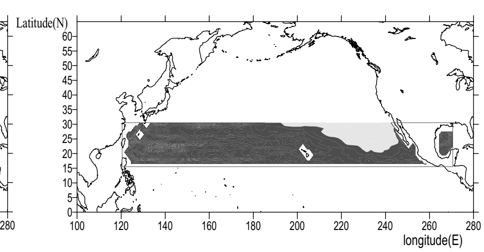

(b) Wave amplification area

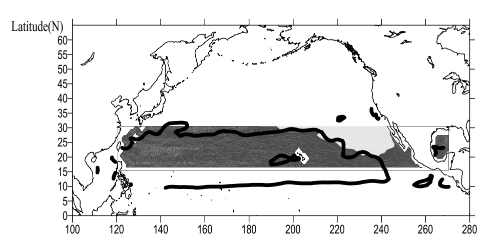

(c) The comparison of the baroclinic instability area and the wave amplification area

Fig. 7. The consistency of the baroclinic instability area and the wave amplification area in the subtropical North Pacific Ocean. The shadow area in (a) shows the baroclinic instability area derived from the Levitus98 data. The shadow area in (b) shows the wave amplification area derived from the TOPEX/POSEIDON altimeter data. The black line in (c) shows the baroclinic instability area and the shadow area in (c) shows the wave amplification area.

need only to determine the layer thickness H_1 and H_2 based on the Levitus98 data. In this paper, we choose $25.0\sigma_\theta$ as the interface between the first layer and the second layer and $27.1\sigma_\theta$ as the interface between the second layer and the third layer. Figure 6 is the potential density field in the 160°E section. From Fig. 6 we can see that our choices of the first and second layer can represent the mixing layer and main thermalcline, and that the determined H_1 and H_2 also agree with those of Liu (1999a, b), Kobashi and Kawamura (2002), Liu *et al.* (2001) and Liu and Pan (2003).

According to the baroclinic instability criterion (10), we can get the baroclinic instability area after determining the layer thicknesses. Figure 7(a) is the baroclinic instability area in the subtropical North Pacific Ocean, derived from the Levitus98 data. Figure 7(b) is the amplification area of the intraseasonal long Rossby wave in the subtropical North Pacific Ocean, derived from the TOPEX/POSEIDON altimeter data. Figure 7(c) is a comparison between the baroclinic instability area and the wave amplification area. From Fig. 7 we can see that in the subtropical North Pacific Ocean, the baroclinic instability area agrees well with the wave amplification area, and this in turn proves that the amplification mechanism of the intraseasonal long Rossby wave in the subtropical ocean is indeed the baroclinic instability.

Figure 8 is a comparison between the baroclinic instability area and the wave amplification area as in Fig. 7(c) in the subtropical North Atlantic Ocean, and this also proves the consistency of the baroclinic instability area with the wave amplification area in the subtropical ocean.

The layer thicknesses, H_1 and H_2, are important in determining the baroclinic instability area in the ocean and our choices of the layer interface do have some uncertainty. To justify our choices, we also choose the potential density layer from $24.8\sigma_\theta$ to $25.2\sigma_\theta$ as the interface between the first layer and the second layer, the potential density layer from $27.0\sigma_\theta$ to $27.2\sigma_\theta$ as the interface between the second layer and the third layer. All these baroclinic instability areas, derived from different density interface, are nearly the same as shown in Figs. 7 and 8 in the subtropical ocean.

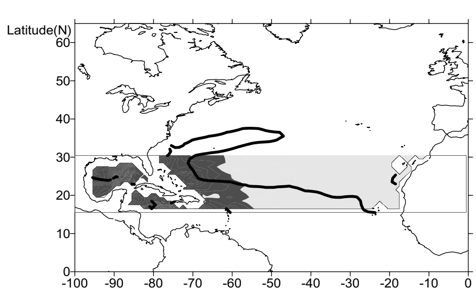

Fig. 8. The consistency of the baroclinic instability area and the wave amplification area in the subtropical North Atlantic Ocean. as in Fig. 7(c) the shadow area shows the wave amplification area and the black line shows the baroclinic instability area.

4. The Interpretation of the Difference between the Wave Amplification Areas of the North Pacific Ocean and the North Atlantic Ocean

In Sections 2 and 3 we prove that the baroclinic instability is the amplification mechanism of the intraseasonal long Rossby wave in the subtropical ocean and the intraseasonal long Rossby wave is amplified in the baroclinic instability area. From Figs. 7 and 8 we can also see that the wave amplification area in the subtropical North Pacific Ocean is very large, covering more than half of the subtropical Pacific Ocean, but the wave amplification area in the subtropical North Atlantic Ocean is only limited in a very small area near the western boundary (that can also be seen from Fig. 2). This means that the baroclinic instability area is large in the subtropical North Pacific Ocean and small in the subtropical North Atlantic Ocean. Why is there an obvious difference in these two oceans? In this section we will first prove the consistency of the baroclinic instability area with the PV pool in the subtropical ocean and secondly, answer the question why there is obvious difference between the wave amplification areas of the North Pacific Ocean and the North Atlantic Ocean.

4.1 The PV homogenization theory

Rhines and Young (1982a, b) have put forward a homogenization PV theory for the first time. In their study they found if the wind forcing is strong enough, the geostrophic contours could be closed in the main thermalcline and be irrelevant to the eastern boundary condition. In this closed geostrophic contours, the PV is uniform, the streamline is also closed and there could exit movement. Now we called this area the homogenous PV pool or the PV pool. Because the PV is nearly uniform in the PV pool and has the same order of the PV gridient out of the PV pool, compared with the planetary PV gridient β, we can use the zero PV gredient to determine the range of the PV pool.

Pedlosky (1996) has studied the homogenization process of the PV in the PV pool using the two and half layer model. In his study he proved that the criterion for determining the PV pool boundary in the second layer was the vanishment of meridianal PV gredient ($\pi_{2y} = 0$), which could prevent the entering of long Rossby wave that carried the information of eastern boundary condition. So we can determine the PV pool with the line of $\pi_{2y} = 0$.

4.2 The consistency of PV pool with the baroclinic instability area in the subtropical ocean

Figure 9 is the distribution of meridianal PV gradient (π_{1y} and π_{2y}) in the first and second layers in the subtropical North Pacific Ocean. The shadow area in Fig. 9 represents negative PV gradient, determined by the boundary of zero PV gradient. From Fig. 9 we can see that in the subtropical North Pacific Ocean the sign of meridianal PV gradient π_{1y} in the first layer is basically positive. According to the baroclinic criterion (10) ($\pi_{1y}\pi_{2y} < 0$), the baroclinic instability area in the subtropical North Pacific Ocean locates at the place where the sign of meridianal PV gradient π_{2y} in the second layer is negative. So the baroclinic instability area can be determined with the line of $\pi_{2y} = 0$ as shown in Fig. 9(b), this is the same as the criterion of the PV pool in the subtropical ocean.

In Rhines and Young (1982a, b), they pointed out that the friction caused the motion in the PV pool and their friction was determined with the vertical velocity shear. As we know vertical velocity shear is related to the baroclinic instability and we can infer that the baroclinic instability is essential in the formation of the PV pool. Pedlosky (1996) also pointed out that the equivalence of the conditions for closed geostrophic contours and the criterion for baroclinic instability satisfyingly identifies the mechanism for the production of motion with the necessary condition for the existence of that motion. When the motion is allowed, the advent of baroclinic instability is capable of producing it.

All the above mentioned show that in the two and half layer model the baroclinic instability area is consistent with the PV pool. But in the real ocean, does the consistency exist?

Figure 10(a) is the averaged geotrophic streamline in the main thermalcline, derived from the Levitus98 data. The black triangles show the outcrop line and the shadow area shows the PV pool, where the geotrophic streamline is closed in the western part of subtropical ocean. Figure 10(b) is the averaged energy transformation rate in the main thermalcline through the baroclinic instability process. According to Gent and Mc Williams (1990), the transformation rate is calculated as follows

$$-gk_{th}\frac{\nabla\rho\bullet\nabla\rho}{\rho_z},$$

where $k_{th} = 1000$ m^2/s, $\rho_z = \partial\rho/\partial z$.

The shadow area in Fig. 10(b) represents the location with high-energy transformation rate, which means the baroclinic instability is strong there.

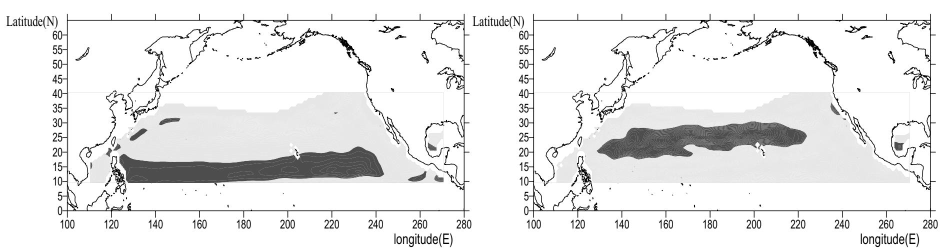

(a) The distribution of π_{1y} (b) The distribution of π_{2y}

Fig. 9. The distribution of meridianal PV gradient in the first layer (a) and the second layer (b). The shadow areas in (a) and (b) have the negative value.

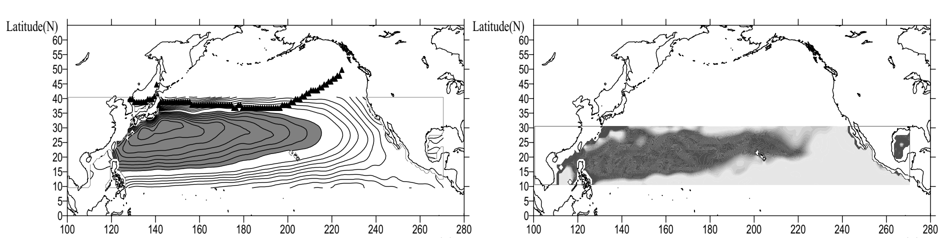

(a) The averaged geotrophic streamline (b) The averaged energy translation rate

Fig. 10. The consistency of the PV pool and the baroclinic instability area in the subtropical ocean. The black triangles in (a) show the outcrop line and the shadow area shows the PV pool. The shadow area in (b) has the high-energy transformation rate.

Compared Fig. 10(a) with Fig. 10(b), we can see that the baroclinic instability area is consistent with the PV pool in the subtropical ocean. The consistency of the PV pool with the baroclinic instability area in the subtropical ocean also means that the intraseasonal long Rossby wave is amplified in the PV pool.

4.3 The reason for the difference between the wave amplification areas of the North Pacific Ocean and the North Atlantic Ocean

From Subsection 4.2 we know that the intraseasonal long Rossby wave is amplified in the PV pool in the subtropical ocean, and where there is also the baroclinic instability area. The difference between the wave amplification areas of the North Pacific Ocean and the North Atlantic Ocean is caused by the different PV pool in these two oceans. So the remaining question here is why the PV pool is so large in the North Pacific Ocean and so small in the North Atlantic Ocean.

Pedlosky (1996) gave the PV pool criterion, determined by the wind forcing as follows

$$x_e - x_r = \frac{\beta^2 H}{f_0 \hat{F}\left(\partial w_E / \partial y\right)_{y=L}}. \tag{13}$$

Where X_e is the position of the eastern boundary and X_r is the position of the PV pool boundary. From this criterion we can see that the distance between the PV pool and the eastern boundary is mainly determined by the wind forcing and vertical structure. If we suppose the wind forcing and vertical structure are equal in the North Pacific Ocean and the North Atlantic Ocean, the distance between the PV pool and the eastern boundary is also equal in these two oceans. Under this hypothesis the PV pool in the North Pacific Ocean will be much larger than that in the North Atlantic Ocean due to the relatively large ocean basin.

Moreover, Pedlosky (1996) also pointed out that the ventilation in a potential density layer could reduce the PV pool. The stronger the ventilation was, the smaller the PV pool would be. As we know the ventilation is very strong in the North Atlantic Ocean, but is weak in the North Pacific Ocean, and this could make the PV pool much smaller in the North Atlantic Ocean than in the North Pacific Ocean.

The intraseasonal long Rossby wave is amplified in the PV pool in the subtropical ocean. Because the PV pool is much larger in the North Pacific Ocean than in the North Atlantic Ocean, the wave amplification area is also much larger in the North Pacific Ocean than in the North Atlantic Ocean. On the other hand, the success in interpreting the difference between the wave amplification areas of these two oceans also proves the validity of baroclinic as the wave amplification mechanism, derived from Sections 2 and 3.

5. Conclusion

In this paper, we have discussed the amplification mechanism of the intraseasonal long Rossby wave in the subtropical ocean. Our conclusion is that the baroclinic instability is the main amplification mechanism of the intraseasonal long Rossby wave in the subtropical ocean. We have also discussed the consistency of the PV pool with the baroclinic instability area in the subtropical ocean, and thus, we can infer that the intraseasonal long Rossby wave is amplified in the PV pool. Because the relatively large ocean basin and weak ventilation, the PV pool is larger in the North Pacific Ocean than in the North Atlantic Ocean. This is the reason why the wave amplification areas are much different in these two oceans.

Acknowledgements

This study was supported by the National Basic Research Priorities Program under contract No. 2002CCA00200, the Key Program of National Natural Science Fund of China under contract No. 40333030 and the Key Project of Chinese Ministry of Education under contract No. 99075 and 104203.

References

Chelton, D. B. and M. G. Schlax (1996): Global observations of oceanic Rossby wave. *Science*, **272**, 234–238.

Chen, H.-y., F.-l. Qiao and Y.-g. Wang (2003): Zonal propagation velocity distribution characteristics of oceanic Rossby waves. *Advances in Marine Science*, **21**(4), 387–392.

Chu, P. C., J. Lan and C. W. Fan (2001): Japan East Sea (JES) circulation and thermohaline structure, Part 2: A variational P-vector method. *J. Phys. Oceanogr.*, **31**, 2886–2902.

De Szoeke, R. A. and D. B. Chelton (1999): The modification of long planetary waves by homogeneous potential vorticity layers. *J. Phys. Oceanogr.*, **29**, 500–511.

Fu, L. L. and B. Qiu (2002): Low-frequency variability of North Pacific Ocean: The roles of boundary- and wind-driven baroclinic Rossby waves. *J. Geophys. Res.*, **107**, 13-1–13-10.

Gent, P. R. and J. C. Mc Williams (1990): Isopycnal mixing in ocean circulation models. *J. Phys. Oceanogr.*, **20**, 150–155.

Hu, Ruijin and Q. Liu (2002): Wavelet of sea surface height intraseasonal oscillation in tropical Pacific. *Oceanologica et Limnologia Sinica*, **33**(3), 303–313 (in Chinese).

Killworth, P. D., D. B. Chelton and R. A. de Szoeke (1997): The speed of observed and theoretical long extratropical planetary wave. *J. Phys. Oceanogr.*, **27**, 1946–1966.

Kobashi, F. and H. Kawamura (2002): Seasonal variation and instability nature of the north Pacific subtropical countercurrent and the Hawaiian Lee countercurrent. *J. Geophys. Res.*, **107**, 6-1–6-18.

Liu, Q.-y. and A.-j. Pan (2003): Intraseasonal oscillation an baroclinic instability of upper layer ocean in the North Equator Current. *Oceanologica et Limnologia Sinica*, **34**, 94–

100 (in Chinese).
Liu, Q.-y. and Q. Wang (1999): Spatial distribution of the sea surface height intraseasonal osciallation in the tropical Pacific. *J. Ocean University of Qingdao*, **29**(4), 549–555 (in Chinese).
Liu, Q.-y., Z.-y. Liu, S.-x. Wang *et al.* (2001): Dynamic features of long Rossby wave in the North Pacific subtropical countercurrent. *Chinese J. Geophys.*, **44**, 28–37.
Liu, Z.-y. (1999a): Planetary wave modes in the thermocline: Non-Doppler-Shift mode, advective mode and Green mode. *Q. J. R. Meteorol. Soc.*, **125**, 1315–1339.
Liu, Z.-y. (1999b): Forced planetary wave response in a thermalcline gyre. *J. Phys. Oceanogr.*, **29**, 1036–1055.
Mitchum, G. T. (1995): The source of 90-day oscillations at Wake Island. *J. Geophys. Res.*, **100**(C2), 2459–2475.
Pedlosky, J. (1987): *Geophysical Fluid Dynamics*. Springer-Verlag, New York.
Pedlosky, J. (1996): *Ocean Circulation Theory*. Springer-Verlag, New York.
Qiao, F.-l., E. Tal and Y.-l. Yuan (2004): On the zonal distribution of high frequency oscillations in the global ocean obtained from altimeter data. *Acta Oceanologica Sinica*, **23**(1), 91–96.
Qiu, B. (1999): Seasonal eddy field modulation of the north Pacific subtropical countercurrent: TOPEX/POSEIDON observations and theory. *J. Phys. Oceanogr.*, **29**, 2471–2486.
Qiu, B., W. Miao and P. Muller (1997): Propagation and decay of forced and free Rossby waves in off-Equatorial ocean. *J. Phys. Oceanogr.*, **27**, 2405–2417.
Rhines, P. B. and W. R. Young (1982a): A theory of the wind-driven circulation. I. Mid-ocean gyres. *J. Fluid Mech.*, **40** (Suppl.), 559–596.
Rhines, P. B. and W. R. Young (1982b): Homogenization of potential vorticity in planetary gyres. *J. Fluid Mech.*, **122**, 347–367.
Stammer, D. (1997): Global characteristics of ocean variability estimated from regional TOPEX/POSEIDON altimeter measurements. *J. Phys. Oceanogr.*, **27**, 1743–1769.
White, W. B., Y. Chao and C.-K. Tai (1998): Coupling of biennial oceanic Rossby waves with the overlying atmosphere in the Pacific basin. *J. Phys. Oceanogr.*, **28**, 1236–1251.